Nanoscale

RSC Publishing

COMMUNICATION

View Article Online
View Journal | View Issue

Cite this: *Nanoscale*, 2013, **5**, 5752

Few-layered $CoHPO_4 \cdot 3H_2O$ ultrathin nanosheets for high performance of electrode materials for supercapacitors†

Received 26th March 2013
Accepted 4th May 2013

DOI: 10.1039/c3nr01460f

www.rsc.org/nanoscale

Huan Pang,*[ab] Shaomei Wang,[a] Weifang Shao,[a] Shanshan Zhao,[a] Bo Yan,[a] Xinran Li,[a] Sujuan Li,[a] Jing Chen[a] and Weimin Du[a]

Ultrathin cobalt phosphate ($CoHPO_4 \cdot 3H_2O$) nanosheets are successfully synthesized by a one pot hydrothermal method. Novel $CoHPO_4 \cdot 3H_2O$ ultrathin nanosheets are assembled for constructing the electrodes of supercapacitors. Benefiting from the nanostructures, the as-prepared electrode shows a specific capacitance of 413 F g^{-1}, and no obvious decay even after 3000 charge–discharge cycles. Such a quasi-two-dimensional material is a new kind of supercapacitor electrode material with high performance.

1 Introduction

In the past few years, tremendous attention has been paid to graphene, the thinnest two-dimensional (2D) crystal with exceptional electronic, optical and mechanical properties.[1,2] These outstanding properties of graphene, due to its atomic-layer thickness and 2D morphology, have encouraged the exploration of other kinds of 2D nanomaterials, derived from layered bulk crystals analogous to graphite.[3–5] After the discovery of the exotic properties of graphene, 2D layered materials, such as metal chalcogenides, transition metal oxides, and other 2D compounds, have gained renewed interest.[6–18] These materials span the wide range of electronic structures, from insulator to metal, and display interesting properties. These include the topological insulator effect,[19,20] superconductivity,[21] and thermoelectricity.[22] Furthermore, a strong interest in group-IV graphene-like 2D buckled nanosheets has recently emerged, namely silicene and germanene.[23–25]

As a result of their distinct properties and high specific surface areas, these 2D materials occupy an important place in various applications, such as optoelectronics, spintronics, catalysts, chemical and biological sensors, supercapacitors, solar cells, and lithium ion batteries.[26–42] Prof. Xie *et al.* have successfully reported highly conductive VS_2 ultrathin films with a high specific capacitance, showing promising signs for this new 2D material to be utilized in energy storage devices.[43]

Metal phosphates exhibit broad and potential applications in many fields.[44–47] A preparation process has been used to synthesize an array of transition metal phosphate amorphous colloidal spheres by Li *et al.*[44] Metal phosphates, especially for layered metal phosphates and phosphonates, have been studied in the years 1987–1990.[48,49] Recently, cobalt phosphate as a kind of a transition metal phosphate has been used as a promising positive electrode for rechargeable ion batteries, heterogeneous catalysts, sorbents, ion exchangers, and magnetism materials due to the layers of connected CoO_x and PO_4 polyhedra, the structures of known zeolite types, and the outstanding electronic or magnetic property.[50–55] However, there are nearly no reports on synthesis and application of cobalt phosphate ultrathin nanosheets.

Herein, we report that a kind of ultrathin cobalt phosphate ($CoHPO_4 \cdot 3H_2O$) nanosheets has been successfully synthesized by a one pot hydrothermal method without any exfoliating. More importantly, novel $CoHPO_4 \cdot 3H_2O$ ultrathin nanosheets were successfully assembled for constructing the electrodes of supercapacitors. As expected, a specific capacitance of 413 F g^{-1} was realized here, no obvious degradation of which was observed even after 3000 charge–discharge cycles, offering a new kind of electrode materials for supercapacitors with high performance based on quasi-two-dimensional materials.

2 Results and discussion

Fig. 1 shows XRD patterns of as-prepared samples. All peaks of the patterns are indexed to be in agreement with $CoHPO_4 \cdot 3H_2O$ (JCPDS no. 39-0702). No peaks of other phosphites or phosphates were detected from these patterns. The peaks are narrow, which indicates the good crystallinity of the as-prepared samples. Good crystallinity of $CoHPO_4 \cdot 3H_2O$ might be

[a]*Key Laboratory for Clearer Energy and Functional Materials of Henan Province, College of Chemistry and Chemical Engineering, Anyang Normal University, Anyang, 455000 Henan, P.R. China*

[b]*State Key Laboratory of Coordination Chemistry, Nanjing University, Nanjing, 210093, Jiangsu, P.R. China. E-mail: huanpangchem@hotmail.com*

† Electronic supplementary information (ESI) available. See DOI: 10.1039/c3nr01460f

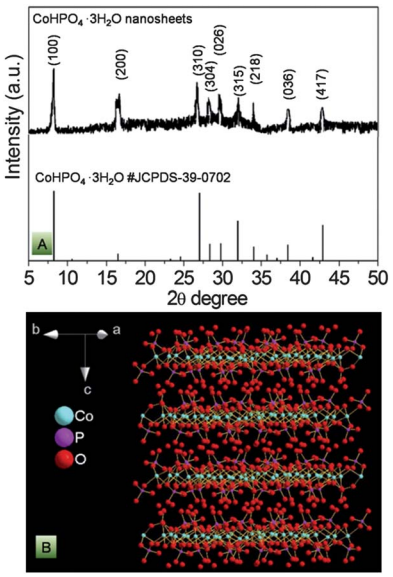

Fig. 1 (A) XRD patterns of as-prepared samples and JCPDS-39-0702; (B) the schematic crystal structures of $CoHPO_4 \cdot 3H_2O$ super cells ($2 \times 2 \times 2$ slabs) projected based on data of ICSD-86668.

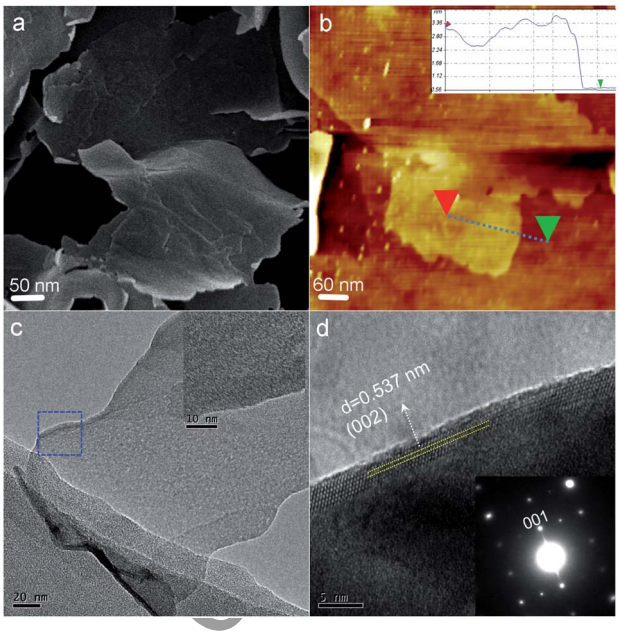

Fig. 2 (a) SEM image of as-prepared $CoHPO_4 \cdot 3H_2O$; (b) AFM image; (c) TEM image; (d) HRTEM image from the magnification of the section marked in (c) and its corresponding SAED pattern.

good to improve the cycle life of electrodes for its stable structure, and it is not easy to be destroyed during the electrochemical process. In Fig. 1B, the schematic crystal structures of $CoHPO_4 \cdot 3H_2O$ super cells ($2 \times 2 \times 2$ slabs) are projected based on data of Inorganic Crystal Structure Data (ICSD)-86668. $CoHPO_4 \cdot 3H_2O$ has the layered crystal structure and such a layered crystal structure might offer many nanochannels and improve diffusion of ions and the electrolyte.

The morphology of as-prepared $CoHPO_4 \cdot 3H_2O$ was examined by field emission scanning electron microscopy (FESEM), atomic force microscopy (AFM) and transmission electron microscopy (TEM). A typical low-magnification SEM image in Fig. 2a shows that the morphology of samples is ultrathin nanosheet in the 2D microscale. The thickness of an ultrathin nanosheet is measured by AFM shown in Fig. 2b. From AFM results, the thickness of the ultrathin nanosheet is ~2.7 nm. And the width of the ultrathin nanosheet is more than 6.0 μm. In addition, there are nearly no pores seen from the HRTEM image in the inset of Fig. 2c. From the HRTEM image of the edge of a nanosheet (Fig. 2d), the ultrathin nanosheet thickness of ~2.7 nm is also directly determined, and is consistent with the AFM measurement in Fig. 2b. The measured distance of neighboring lattice fringes in Fig. 2d is ~0.537 nm, corresponding well to the (002) lattice spacing of $CoHPO_4 \cdot 3H_2O$. It denotes that the $CoHPO_4 \cdot 3H_2O$ ultrathin nanosheet is comprised of 4–5 single layers. The selected area electron diffraction (SAED) pattern is shown in the inset of Fig. 2d, which demonstrates the good crystalline nature of the product and may be described as a single crystal with [001] growth direction. A schematic illustration of the layered stacking of the synthetic $CoHPO_4 \cdot 3H_2O$ ultrathin nanosheets is shown in Scheme 1; it clearly exhibits a few layered $CoHPO_4 \cdot 3H_2O$ ultrathin nanosheet model image.

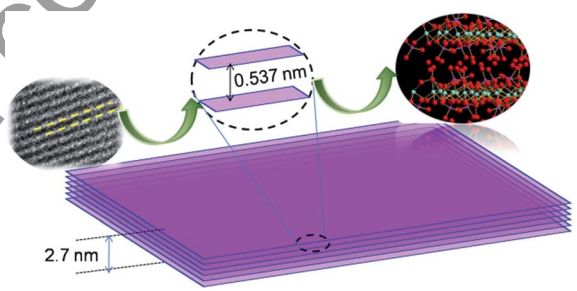

Scheme 1 A few layered $CoHPO_4 \cdot 3H_2O$ ultrathin nanosheet model image.

We also explored the possible formation process of $CoHPO_4 \cdot 3H_2O$ ultrathin nanosheets, and found that the reaction time affected the morphology of the product. The product was synthesized under different hydrothermal conditions (seen in ESI Fig. 1†). As can been seen in ESI Fig. 1a,† quantum dots were obtained under hydrothermal conditions for 2 days. After being

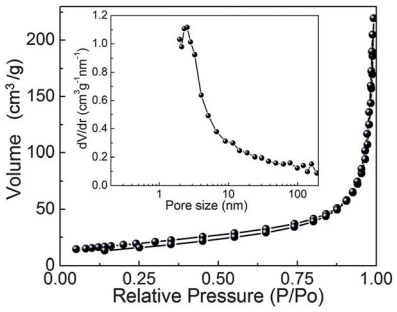

Fig. 3 N_2 adsorption–desorption isotherms of $CoHPO_4 \cdot 3H_2O$ ultrathin nanosheets, and the inset shows the pore-size distribution curve.

hydrothermal conditions for 4 days, nanonetworks were obtained as shown in ESI Fig. 1b.† And after 6 days under hydrothermal conditions, $CoHPO_4 \cdot 3H_2O$ ultrathin nanosheets were successfully synthesized as shown in ESI Fig. 1c.† When further maintained for 8 days, these $CoHPO_4 \cdot 3H_2O$ ultrathin nanosheets assembled again and formed a larger one as shown in ESI Fig. 1d.† ESI Fig. 2† shows that a phase evolution occurred during this process. The product obtained after 2 hours is an amorphous material. On prolonging the reaction to 4 hours, the phase of $CoHPO_4 \cdot 3H_2O$ is found and some amorphous materials existed. And we find that EG plays a key role in the formation of the layered structures. The crystallization and reconstruction of $CoHPO_4 \cdot 3H_2O$ are effected by EG molecules.[50,51] In a previous work, $Co_{11}(HPO_3)_8(OH)_6$ microarchitectures (seen in ESI Fig. 3†) were obtained by using 20 mL deionized water instead of EG.

To gain further insight into the specific surface area of $CoHPO_4 \cdot 3H_2O$ ultrathin nanosheets, Brunauer–Emmett–Teller (BET) measurements were performed. And the N_2 adsorption–desorption isotherms of $CoHPO_4 \cdot 3H_2O$ ultrathin nanosheets are shown in Fig. 3. The BET surface area of $CoHPO_4 \cdot 3H_2O$ ultrathin nanosheets is 267 $m^2\ g^{-1}$. The pore-size distribution (in the inset of Fig. 3) was determined by using the Barrett–Joyner–Halenda (BJH) method from the desorption branch of the isotherm. The average pore diameter of the sample is 2–6 nm, which is attributed to the layered structures assembled or folded. As widely reported, a high surface area and layered ultrathin nanosheets usually offer many nanochannels for contacting the electrolyte with surface-interfaces of novel micro/nanostructures.[43]

Cyclic voltammogram (CV) studies were employed to characterize the capacitive performances of $CoHPO_4 \cdot 3H_2O$ ultrathin

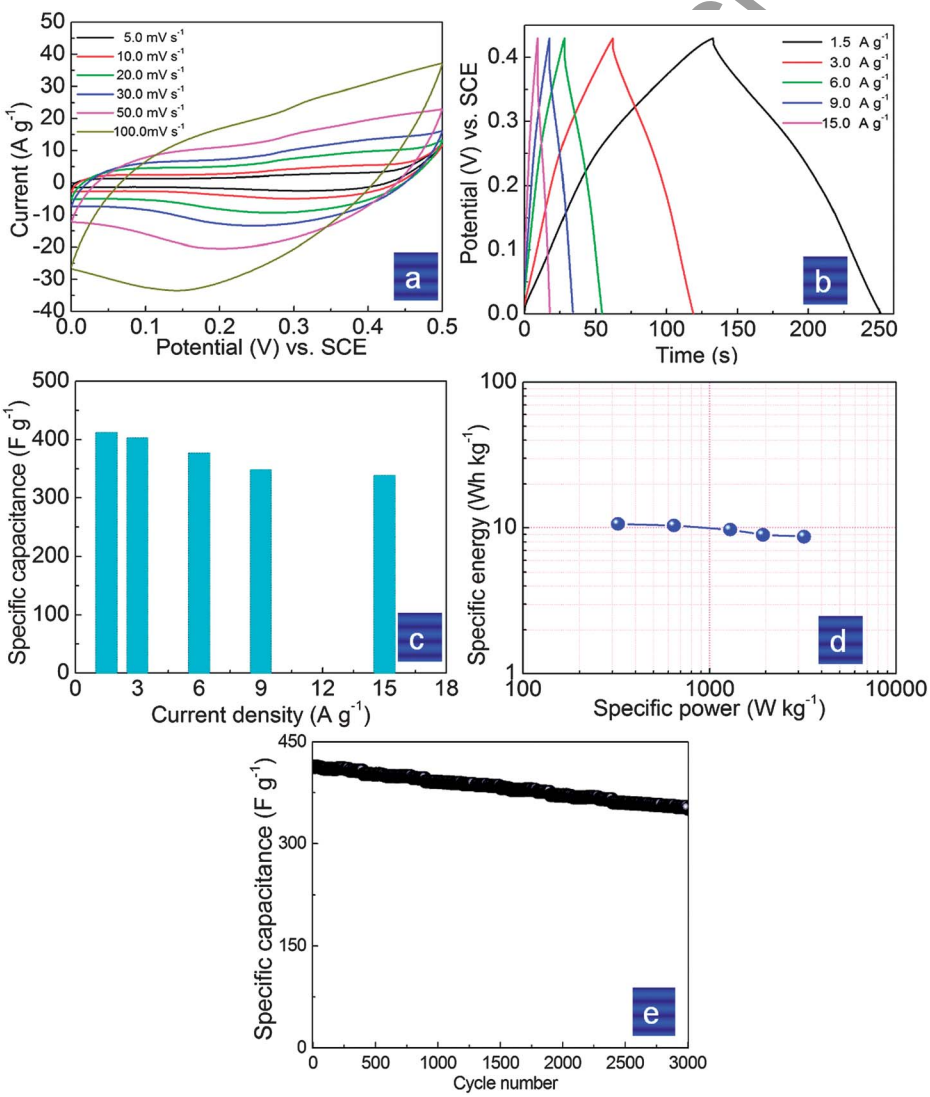

Fig. 4 (a) Cyclic voltammetry experiments within a 0.0–0.50 V range at a scan rate of 5–100 mV s^{-1} were performed on the layered $CoHPO_4 \cdot 3H_2O$ ultrathin nanosheet electrodes in 3.0 M KOH electrolytes at room temperature, (b) the galvanostatic charge–discharge curves of $CoHPO_4 \cdot 3H_2O$ ultrathin nanosheet electrodes at current densities of 1.5–15.0 A g^{-1} in 3.0 M KOH electrolytes, (c) specific capacitances of $CoHPO_4 \cdot 3H_2O$ ultrathin nanosheet electrodes derived from the discharging curves at the current density of 1.5–15.0 A g^{-1} in 3.0 M KOH electrolytes, (d) a plot of the estimated specific energy and specific power at various charge–discharge rates in 3.0 M KOH electrolytes, and (e) charge–discharge cycling test at the current density of 1.5 A g^{-1} in 3.0 M KOH electrolytes.

nanosheet electrodes. Fig. 4a shows the CVs of $CoHPO_4 \cdot 3H_2O$ ultrathin nanosheet electrodes (a mass loading of ~5 mg) in a 3.0 M KOH electrolyte at different scan rates in the range 5–100 mV s^{-1}. As seen in Fig. 4a, the shapes are different from that of electric double-layer capacitance, suggesting that the capacity mainly results from pseudocapacitive capacitance, and it is clear that the Faradaic pseudocapacitive property of $CoHPO_4 \cdot 3H_2O$ ultrathin nanosheets is based on the surface redox mechanism of Co^{2+} to Co^{3+} at the surface. The CV curves of the compound in a relatively broad voltage window of 0.0–1.0 V are shown in ESI Fig. 4.† It is seen that electrochemical capacitor behavior nearly disappears from 0.5 to 1.0 V.

Chronopotentiometry (CP) curves at different current densities are shown in Fig. 4b. The symmetrical characteristic of charging–discharging curves is good, which means that the $CoHPO_4 \cdot 3H_2O$ ultrathin nanosheet electrodes with excellent electrochemical capability and redox process are reversible. The relationships between the specific capacitances calculated by CP curves and current densities are given in Fig. 4c. Based on the CP curves, $CoHPO_4 \cdot 3H_2O$ ultrathin nanosheet electrodes have a large specific capacitance and reach up to 413 F g^{-1} at a current density of 1.5 A g^{-1}, and remain at 338 F g^{-1} even at 15.0 A g^{-1}. The specific capacitance of $CoHPO_4 \cdot 3H_2O$ ultrathin nanosheets is better than some cobalt based phosphate micro/nanomaterials, such as our previous results – $NH_4CoPO_4 \cdot H_2O$ microflowers (<340 F g^{-1} at 1.5 A g^{-1}),[52] cobalt phosphite ($Co_{11}(HPO_3)_8(OH)_6$) microarchitectures (<312 F g^{-1} at 1.5 A g^{-1}),[53] and cobalt pyrophosphate nano/microstructures (367 F g^{-1} at 0.625 A g^{-1})[54] – but lower than other supercapacitor materials.[55–59]

Specific energy and specific power are the two key factors for evaluating the power applications of electrochemical supercapacitors. A good electrochemical supercapacitor is expected to provide both high energy density and specific capacitance. Fig. 4d shows the plot for $CoHPO_4 \cdot 3H_2O$ ultrathin nanosheet electrodes in a 3.0 M KOH aqueous solution. $CoHPO_4 \cdot 3H_2O$ ultrathin nanosheet electrodes also have good specific energy and specific power. The specific energy of $CoHPO_4 \cdot 3H_2O$ ultrathin nanosheet electrodes decreases from 10.6 to 8.7 W h kg^{-1}, while the specific power increases from 322 to 3225 W kg^{-1} as the galvanostatic charge–discharge current density increases from 1.5 to 15.0 A g^{-1}.

It is very important for electrode materials to have good specific capacitance retention. Supercapacitors should work steadily and safely, which requires the specific capacitance of electrode materials to change as little as possible. The relationships of the specific capacitance with cycling number of $CoHPO_4 \cdot 3H_2O$ ultrathin nanosheet electrodes are shown in Fig. 4e. It shows excellent specific capacitance retention under 1.5 A g^{-1}. After 300 continuous charge–discharge cycles, $CoHPO_4 \cdot 3H_2O$ ultrathin nanosheet electrodes almost retain the same specific capacitance as its initial value. More importantly, $CoHPO_4 \cdot 3H_2O$ ultrathin nanosheet electrodes still retain more than 85.1% of their specific capacitance after 3000 continuous charge–discharge cycles.

We proposed two possible mechanisms for the charge–discharge behavior:

$$CoHPO_4 \cdot 3H_2O + OH^- - e^- = CoPO_4 + 4H_2O; \quad (a)$$

$$CoHPO_4 \cdot 3H_2O + K^+ + e^- = KCoHPO_4 + 3H_2O. \quad (b)$$

To identify the exact electrical conductivity of electrodes, we have measured the EIS spectrum of $CoHPO_4 \cdot 3H_2O$ ultrathin nanosheet electrodes at room temperature in the frequency range 0.01 to 10^5 Hz at 0.40 V. Fig. 5 shows the EIS of $CoHPO_4 \cdot 3H_2O$ ultrathin nanosheet electrodes at room temperature and its calculated curve by ZSimpWin software. An equivalent circuit used to fit the impedance curve is given in the inset of Fig. 5a, which is similar to the circuit employed for the working electrode of a supercapacitor. The EIS data can be fitted by a bulk solution resistance R_s, a charge-transfer R_{ct} and a pseudocapacitive element C_p from the redox process of electrode materials, and a CPE to account for the double-layer capacitance. The charge-transfer resistance values R_{ct} of all the samples were calculated by ZSimpWin software. And from the calculated results, we found that the R_{ct} of $CoHPO_4 \cdot 3H_2O$ ultrathin nanosheet electrodes is 8.9 Ω. This clearly demonstrates the reduced charge-transfer resistance of $CoHPO_4 \cdot 3H_2O$ ultrathin nanosheet electrodes. In addition, the charge-transfer resistance R_{ct}, also called Faraday resistance, is a limiting factor for the specific power of the supercapacitor. It is the low Faraday resistance that results in the high specific power of layered

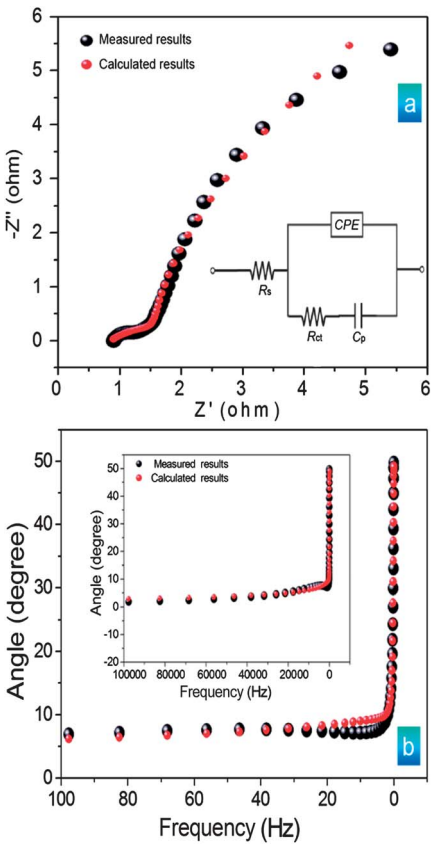

Fig. 5 The electrochemical impedance spectra (EIS) of the electrodes at room temperature and its corresponding calculated curve, in insets of (a) the equivalent circuit for the electrochemical impedance spectrum; and (b) the phase angles for impedance plots and its corresponding calculated curve.

$CoHPO_4 \cdot 3H_2O$ ultrathin nanosheets. This layered structure surface–interface character might also decrease the polarization of the electrode, and thus increase the capacity. The phase angles for impedance plots of $CoHPO_4 \cdot 3H_2O$ ultrathin nanosheet electrodes and their calculated curve by ZSimpWin software are observed in Fig. 5b. These phase angles are nearly 50° in the low frequencies clearly, which means that the $CoHPO_4 \cdot 3H_2O$ ultrathin nanosheets allow ion or electrolyte transfer to occur quickly.

3 Conclusions

In this work, unique $CoHPO_4 \cdot 3H_2O$ ultrathin nanosheets have been successfully synthesized through a hydrothermal method. More importantly, $CoHPO_4 \cdot 3H_2O$ ultrathin nanosheets show a novel layered surface–interface condition, which plays a key role in ion intercalation/extraction into/out and electrolyte access. The measurement of electrochemical properties of $CoHPO_4 \cdot 3H_2O$ ultrathin nanosheets is important work, which successfully illustrates that $CoHPO_4 \cdot 3H_2O$ ultrathin nanosheet materials can be applied as an electroactive material for supercapacitors. Despite specific capacitance of $CoHPO_4 \cdot 3H_2O$ ultrathin nanosheet materials being not much larger than some previous materials,[53–56] it is a good example to prove that physical and chemical properties of nano/microstructured materials are related to their structures, and the precise control of morphology of nanomaterials will serve for controlling the performance. Exploring the electrochemical characteristics of novel nano/micromaterials might direct a new generation of supercapacitor materials.

4 Experimental section

4.1 Synthesis of $CoHPO_4 \cdot 3H_2O$ ultrathin nanosheets

In a typical synthesis, 0.28 g cobalt chloride and 0.30 g sodium pyrophosphate were mixed with 20 mL ethylene glycol. The above mixture was stirred for 1 hour at room temperature. The solution mixture was put in a Teflon-lined stainless steel autoclave and heated at 200.0 °C for 6 days. After the reaction, violet precipitates were obtained. The precipitates were thoroughly washed with distilled water and ethanol to remove ions possibly remaining in the final products, and dried at room temperature in air.

4.2 Electrochemical measurements

Electrochemical study on $CoHPO_4 \cdot 3H_2O$ ultrathin nanosheet electrodes was carried out on a CHI 660D electrochemical working station (Shanghai Chenhua Instrument, Inc.). All electrochemical performances were carried out in a conventional three-electrode system equipped with a platinum electrode and a saturated calomel electrode (SCE) as counter and reference electrodes, respectively. Before electrochemical measurement, we purged out O_2 from the solution with the inert gas Ar. The working electrode was made from mixing of active materials ($CoHPO_4 \cdot 3H_2O$ ultrathin nanosheets), acetylene black, and PTFE (polytetrafluoroethylene) with a weight ratio of 80 : 15 : 5, coating on a piece of foamed nickel foam of about 1 cm^2, and pressing it to be a thin foil at a pressure of 5.0 MPa. The electrolyte was a 3.0 M KOH solution. Cyclic voltammetry and galvanostatic charge–discharge methods were used to investigate capacitive properties of $CoHPO_4 \cdot 3H_2O$ ultrathin nanosheet electrodes. And electrochemical impedance spectroscopy measurements of all the samples were conducted at 0.40 V in the frequency range of 100 kHz to 0.01 Hz with an AC voltage amplitude of 5 mV by using PARSTAT2273.

4.3 Characterizations

The morphology of as-prepared samples was observed by a JEOL JSM-6701F field-emission scanning electron microscope (FE-SEM) at an acceleration voltage of 5.0 kV. The phase analyses of the samples were performed by X-ray diffraction (XRD) on a Rigaku-Ultima III with Cu K_α radiation ($\lambda = 1.5418$ Å). Nitrogen adsorption–desorption measurements were performed on a Gemini VII 2390 Analyzer at 77 K using the volumetric method. The specific surface area was obtained from the N_2 adsorption–desorption isotherms and was calculated by the Brunauer–Emmett–Teller (BET) method. Transmission electron microscopy (TEM) images and HRTEM images were captured on the JEM-2100 instrument microscope at an acceleration voltage of 200 kV. The atomic force microscope (AFM) image was measured at CSPM4000 (Benyuan, Beijing).

Acknowledgements

This work is supported by the National Natural Science Foundation of China (NSFC 21201010, 21003001 and 21071006), Science and Technology Foundation of Henan Province (122102210253, 13A150019), and China Postdoctoral Science Foundation (2012M521115).

Notes and references

1 K. S. Novoselov, A. K. Geim, S. V. Morozov, D. Jiang, Y. Zhang, S. V. Dubonos, I. V. Grigorieva and A. A. Firsov, *Science*, 2004, **306**, 666–669.
2 X. Huang, Z. Yin, S. Wu, X. Qi, Q. He, Q. Zhang, Q. Yan, F. Boey and H. Zhang, *Small*, 2011, **7**, 1876–1902.
3 K. S. Novoselov, D. Jiang, F. Schedin, T. J. Booth, V. V. Khotkevich, S. V. Morozov and A. K. Geim, *Proc. Natl. Acad. Sci. U. S. A.*, 2005, **102**, 10451–10453.
4 H. Matte, A. Gomathi, A. K. Manna, D. J. Late, R. Datta, S. K. Pati and C. N. R. Rao, *Angew. Chem., Int. Ed.*, 2010, **49**, 4059–4062.
5 Z. Y. Zeng, Z. Y. Yin, X. Huang, H. Li, Q. Y. He, G. Lu, F. Boey and H. Zhang, *Angew. Chem., Int. Ed.*, 2011, **50**, 11093–11097.
6 J. A. Wilson and A. D. Yoffe, *Adv. Phys.*, 1969, **18**, 193.
7 J. N. Coleman, M. Lotya, A. O'Neill, S. D. Bergin, P. J. King, U. Khan, K. Young, A. Gaucher, S. De, R. J. Smith, I. V. Shvets, S. K. Arora, G. Stanton, H. Y. Kim, K. Lee, G. T. Kim, G. S. Duesberg, T. Hallam, J. J. Boland, J. J. Wang, J. F. Donegan, J. C. Grunlan, G. Moriarty, A. Shmeliov, R. J. Nicholls, J. M. Perkins, E. M. Grieveson, K. Theuwissen, D. W. McComb, P. D. Nellist and V. Nicolosi, *Science*, 2011, **331**, 568–571.

8 W. J. Zhou, Z. Y. Yin, Y. P. Du, X. Huang, Z. Y. Zeng, Z. X. Fan, H. Liu, J. Y. Wang and H. Zhang, *Small*, 2013, **9**, 140–147.
9 Z. Zeng, T. Sun, J. Zhu, X. Huang, Z. Yin, G. Lu, Z. Fan, Q. Yan, H. H. Hng and H. Zhang, *Angew. Chem., Int. Ed.*, 2012, **51**, 9052–9056.
10 A. Splendiani, L. Sun, Y. B. Zhang, T. S. Li, J. Kim, C. Y. Chim, G. Galli and F. Wang, *Nano Lett.*, 2010, **10**, 1271–1275.
11 Y. J. Zhang, J. T. Ye, Y. Matsuhashi and Y. Iwasa, *Nano Lett.*, 2012, **12**, 1136–1140.
12 X. Huang, Z. Y. Zeng, S. Y. Bao, M. F. Wang, X. Y. Qi, Z. X. Fan and H. Zhang, *Nat. Commun.*, 2013, **4**, 1444.
13 Y. F. Sun, Z. Sun, S. Gao, H. Cheng, Q. Liu, J. Piao, T. Yao, C. Z. Wu, S. Hu, S. Q. Wei and Y. Xie, *Nat. Commun.*, 2012, **3**, 1057.
14 M. Osada and T. Sasaki, *Adv. Mater.*, 2012, **24**, 210.
15 L. Hozoi, L. Siurakshina, P. Fulde and J. van der Brink, *Sci. Rep.*, 2011, **1**, 65.
16 D. Golberg, Y. Bando, Y. Huang, T. Terao, M. Mitome, C. C. Tang and C. Y. Zhi, *ACS Nano*, 2010, **4**, 2979.
17 H. J. Zhang, C. X. Liu, X. L. Qi, X. Dai, Z. Fang and S. C. Zhang, *Nat. Phys.*, 2009, **5**, 438.
18 H. Tao, D. Liang, R. L. Qiu and X. P. A. Gao, *ACS Nano*, 2011, **5**, 7510.
19 M. R. Lang, L. He, F. X. Xiu, X. X. Yu, J. X. Tang, Y. Wang, X. F. Kou, W. J. Jiang, A. V. Fedorov and K. L. Wang, *ACS Nano*, 2012, **6**, 295.
20 H. B. Zhang, H. L. Yu, D. H. Bao, S. W. Li, C. X. Wang and G. W. Yang, *Adv. Mater.*, 2012, **24**, 132.
21 F. R. Gamble and B. G. Silbernagel, *J. Chem. Phys.*, 1975, **63**, 2544.
22 X. F. Tang, W. J. Xie, H. Li, W. Y. Zhao, Q. J. Zhang and M. Niino, *Appl. Phys. Lett.*, 2007, **90**, 012102.
23 K. Takeda and K. Shiraishi, *Phys. Rev. B: Condens. Matter Mater. Phys.*, 1994, **50**, 14916.
24 B. Aufray, A. Kara, S. Vizzini, H. Oughaddou, C. Léandri, B. Ealet and G. Le Lay, *Appl. Phys. Lett.*, 2010, **96**, 183102.
25 S. Cahangirov, M. Topsakal, E. Aktürk, H. Şahin and S. Ciraci, *Phys. Rev. Lett.*, 2009, **102**, 236804.
26 Y. Li, H. Wang, L. Xie, Y. Liang, G. Hong and H. Dai, *J. Am. Chem. Soc.*, 2011, **133**, 7296–7299.
27 J. Kibsgaard, Z. Chen, B. N. Reinecke and T. F. Jaramillo, *Nat. Mater.*, 2012, **11**, 963–969.
28 B. Radisavljevic, M. B. Whitwick and A. Kis, *ACS Nano*, 2011, **5**, 9934.
29 S. J. Ding, D. Y. Zhang, J. S. Chen and X. W. Lou, *Nanoscale*, 2012, **4**, 95.
30 X. D. Zhang, J. J. Zhang, J. Y. Zhao, B. C. Pan, M. G. Kong, J. Chen and Y. Xie, *J. Am. Chem. Soc.*, 2012, **134**, 11908–11911.
31 K. F. Mak, C. Lee, J. Hone, J. Shan and T. F. Heinz, *Phys. Rev. Lett.*, 2010, **105**, 136805.
32 T. Li and G. Galli, *J. Phys. Chem. C*, 2007, **111**, 16192–16196.
33 M. M. Benameur, B. Radisavljevic, J. S. Héron, S. Sahoo, H. Berger and A. Kis, *Nanotechnology*, 2011, **22**, 125706.
34 Y. Zhang, T.-T. Tang, C. Girit, Z. Hao, M. C. Martin, A. Zettl, M. F. Crommie, Y. R. Shen and F. Wang, *Nature*, 2009, **459**, 820–823.
35 Y. Yoon, K. Ganapathi and S. Salahuddin, *Nano Lett.*, 2011, **11**, 3768–3773.
36 J. Pu, Y. Yomogida, K.-K. Liu, L.-J. Li, Y. Iwasa and T. Takenobu, *Nano Lett.*, 2012, **12**, 4013–4017.
37 S. Kim, A. Konar, W.-S. Hwang, J. H. Lee, J. Lee, J. Yang, C. Jung, H. Kim, J.-B. Yoo, J.-Y. Choi, Y. W. Jin, S. Y. Lee, D. Jena, W. Choi and K. Kim, *Nat. Commun.*, 2012, **3**, 1011.
38 B. Radisavljevic, M. B. Whitwick and A. Kis, *ACS Nano*, 2011, **5**, 9934–9938.
39 H. Wang, L. Yu, Y.-H. Lee, Y. Shi, A. Hsu, M. L. Chin, L.-J. Li, M. Dubey, J. Kong and T. Palacios, *Nano Lett.*, 2012, **12**, 4674–4680.
40 F. Xia, T. Mueller, Y.-M. Lin and P. Avouris, *Nat. Nanotechnol.*, 2009, **4**, 839–843.
41 H. S. Lee, S.-W. Min, Y.-G. Chang, M. K. Park, T. Nam, H. Kim, J. H. Kim, S. Ryu and S. Im, *Nano Lett.*, 2012, **12**, 3695–3700.
42 C. Zhong, C. Duan, F. Huang, H. Wu and Y. Cao, *Chem. Mater.*, 2010, **23**, 326–340.
43 J. Feng, X. Sun, C. Z. Wu, L. L. Peng, C. W. Lin, S. L. Hu, J. L. Yang and Y. Xie, *J. Am. Chem. Soc.*, 2011, **133**, 17832–17838.
44 C. Chen, W. Chen, J. Lu, D. Chu, Z. Huo, Q. Peng and Y. Li, *Angew. Chem., Int. Ed.*, 2009, **48**, 4816.
45 C. Morgovan, E. Marian, A. Iovi, I. Bratu and G. Borodi, *Rev. Chim.*, 2009, **60**, 1282.
46 H. Jiang, T. Zhao, C. Li and J. Ma, *J. Mater. Chem.*, 2011, **21**, 3818.
47 I. S. Cho, D. W. Kim, S. Lee, C. H. Kwak, S. T. Bae, J. H. Noh, S. H. Yoon, H. S. Jung, D. W. Kim and K. S. Hong, *Adv. Funct. Mater.*, 2008, **18**, 2154.
48 N. J. Clayden, *J. Chem. Soc., Dalton Trans.*, 1987, 1877.
49 G. Alberti, M. G. Bernasconi and M. Casciola, *React. Polym.*, 1989, **11**, 245.
50 D. Q. Liu, X. Wang, X. B. Wang, W. Tian, J. W. Liu, C. Y. Zhi, D. Y. He, Y. Bandoa and D. Golberg, *J. Mater. Chem. A*, 2013, **1**, 1952.
51 X. Wang, Y. J. Yang, T. Y. Zhai, Y. T. Zhong, Z. J. Gu, Y. C. Cao, Y. L. Zhao, Y. Ma and J. N. Yao, *Chem.–Eur. J.*, 2013, **19**, 5442.
52 H. Pang, Z. Yan, W. Wang, J. Chen, J. S. Zhang and H. H. Zheng, *Nanoscale*, 2012, **4**, 5946–5953.
53 H. Pang, Y. Y. Liu, J. Li, Y. H. Ma, G. C. Li, Y. N. Ai, J. Chen, J. S. Zhang and H. H. Zheng, *Nanoscale*, 2013, **5**, 503–507.
54 H. Pang, Z. Yan, Y. Ma, G. Li, J. Chen, J. Zhang, W. Du and S. Li, *J. Solid State Electrochem.*, 2013, **17**, 1383.
55 C. Z. Yuan, X. G. Zhang, L. H. Su, B. Gao and L. F. Shen, *J. Mater. Chem.*, 2009, **19**, 5772–5777.
56 Z. Lu, Z. Chang, W. Zhu and X. M. Sun, *Chem. Commun.*, 2011, **47**, 9651–9653.
57 B. Qu, Y. Chen, M. Zhang, L. Hu, D. Lei, B. Lu, Q. Li, Y. Wang, L. Chen and T. H. Wang, *Nanoscale*, 2012, **4**, 7810.
58 C. C. Hu, J. C. Chen and K. H. Chang, *J. Power Sources*, 2013, **221**, 128.
59 H. Pang, C. Z. Wei, Y. H. Ma, S. S. Zhao, G. C. Li, J. S. Zhang, J. Chen and S. J. Li, *ChemPlusChem*, 2013, DOI: 10.1002/cplu.201300015.